TÜBİTAK

Turkish Journal of Chemistry

http://journals.tubitak.gov.tr/chem/

Research Article

Turk J Chem
(2018) 42: 86 – 99

doi:10.3906/kim-1704-12

Adsorption of anionic and cationic dyes on biochars, produced by hydrothermal carbonization of waste biomass: effect of surface functionalization and ionic strength

Ezgi ÇAĞLAR[1], Yusuf Osman DONAR[1], Ali SINAĞ[1,*], İbrahim BİROĞUL[1], Selva BİLGE[1], Kıvanç AYDINCAK[1], Oleksii PLIEKHOV[2]

[1]Department of Chemistry, Faculty of Science, Ankara University, Ankara, Turkey
[2]National Institute of Chemistry, Ljubljana, Slovenia

Received: 06.04.2017 • **Accepted/Published Online:** 19.09.2017 • **Final Version:** 08.02.2018

Abstract: In this work, surface-functionalization agents and various salts as auxiliaries were used to improve the adsorption capacity of biochars produced via hydrothermal carbonization of glucose, cellulose, and hazelnut shell. The effect of surface functionalization with different acids and bases as well as neutral salts on the adsorption of methylene blue and methyl orange was investigated using Boehm titration, Fourier transform infrared spectroscopy, and X-ray photoelectron spectroscopy techniques. Surface functionalization of biochars leads to an increase in the number of oxygen-containing functional groups on the surface, thus increasing the adsorption capacity. To probe the influence of ionic strength on the adsorption process, three auxiliaries, namely potassium chloride, cetyltrimethylammonium bromide, and sodium bicarbonate, were examined. The increase in total electrolyte concentration significantly affected the pH of the solution and as a result electrostatic interactions between dyes and biochars. Dye adsorption capacities reached 234.57 mg/g for methylene blue and 306.13 mg/g for methyl orange in the presence of cellulose-based and NaOH-functionalized biochar and glucose-based H_2SO_4-functionalized biochar, respectively.

Key words: Hydrothermal carbonization, adsorption of dyes, surface functionalization, Boehm titration

1. Introduction

The textile industry is one of the most important industrial sectors of many national economies. However, it consumes considerably high amounts of processed water and produces highly polluted discharge water in large amounts, the cleaning of which has been an issue of major concern for many years. Even very small quantities of organic dyes, which are used in textile factories as well as for production of paper, leather, wool, nylons, polyesters, etc.,[1] can be highly visible and pollutive in water, threatening human and animal health. For example, many health problems such as eye irritation, difficulty in breathing on inhalation, cancer, jaundice, tumors, skin irritation, allergies, heart defects, mutations, etc. were caused by organic dyes.[2] Therefore, these toxic pollutants, which are found in wastewaters, should be removed.

There are several methods for the removal of organic pollutants/dyes from wastewater such as photocatalytic degradation,[3] chemical precipitation,[4] sonochemical degradation,[5] ion exchange,[6] micellar enhanced ultrafiltration,[7] physical adsorption,[8] electrochemical degradation,[9] bioremoval,[10] adsorption/precipitation,[11] integrated chemical/biological degradation,[12] solar photo-Fenton process,[13] and biological process.[14] Among

*Correspondence: sinag@science.ankara.edu.tr

these methods, adsorption techniques have long been used in scientific circles because of their easy handling, high efficiency, economic feasibility, and simplicity in design.[1]

Activated carbon is a well-known commercial material that is effectively used as an adsorbent for removal of a wide variety of organic and inorganic pollutants dissolved in water. However, production of activated carbon requires high temperature and an additional activation process.[15,16] Comparatively, owing to chemical or steam activation, activated carbon is a much more expensive material than biochar. Biochar may therefore be a cost-effective material.[17–21] The most appropriate method for biochar production is hydrothermal carbonization, which enables control of the carbonization process and its chemistry as well as morphology and particle size.[22,23] In addition, feedstocks for biochar production are mainly supplied from agricultural solid waste biomass and are abundant and of low cost.[24–27]

The main objective of the present study was to evaluate the effect of surface functionalization and ionic strength on the adsorption process of anionic and cationic dyes on biochars, produced by hydrothermal carbonization of model and real biomasses. Cellulose (C) is the one of the primary component of the real biomass (27.3%)[28] and glucose (G) was chosen as the building block of cellulose, while hazelnut shell (HS) was selected as the real biomass. The surface of the biochars was functionalized using HCl, NaOH, $(NH_4)_2SO_4$, H_2SO_4, and NH_3 for investigating the effect of functional groups on the adsorption behavior. Various instrumental and analytical techniques such as Brunauer–Emmett–Teller N_2 adsorption, X-ray photoelectron spectroscopy, Fourier transform infrared spectroscopy, and Boehm titration were employed to reveal the surface chemistry. Two organic dyes, methylene blue (MB) and methyl orange (MO), and three auxiliaries (CTAB, $NaHCO_3$, and KCl) were used as model compounds to investigate the usage of biochars as adsorbents in single-system adsorption of dyes.

2. Results and discussion

2.1. Product yields

Under determined conditions, the product yields obtained from glucose, cellulose, and hazelnut shells were 39.3%, 68.8%, and 47.1%, respectively. The carbon-based biochars were denoted as GHTC, CHTC, and HSHTC, respectively. The product yields of biochar revealed a wide range diversity due to the different formation mechanism pathways resulting from the solubility of the raw material.

2.2. Chemical characterization of BC

Figure 1 shows the FTIR spectra of the hydrothermally carbonized and raw biomasses. The band at about 3240 cm^{-1} indicates OH groups in the glucose structure. This sharp peak disappears in the case of GHTC, and a wide peak within the 3000–3700 cm^{-1} band is observed. This peak indicates the formation of carbonyl groups derived from the OH regions. Unlike the untreated glucose, the peak at 1700 cm^{-1} obtained for the biochar (GHTC) indicates the presence of carbonyl, ester, quinine, and carboxylic groups because of the C=O vibrations.[29] The presence of C=O stretching vibrations is also evidence of the presence of secondary bands at 2324 and 2350 cm^{-1}. Glucose has an aliphatic structure (C–H stretching) as can be deduced from the band at 2900–2975 cm^{-1}. However, the intensity of this peak is reduced in GHTC. The existence of aromatic rings is shown by the band at 1620 cm^{-1}, attributed to C=C vibrations and to the bands in the 875–750 cm^{-1} region, assigned to aromatic C–H out-of-plane bending vibrations.[30,31] Moreover, it is thought that alkyl groups are degraded after a certain temperature due to their low thermal stability. The bands in the 1000–1400 cm^{-1}

region correspond to C–O stretching, whereas the bands at 3300 cm^{-1} can be attributed to C–OH vibrations. The band at 2900 cm^{-1} can be assigned to the aliphatic fragment in the untreated cellulose.[32] Due to an increase in temperature from 220 to 260 °C, OH groups, aliphatic groups, and C–O stretching (etheric bonds) were broken partially. C=O stretching vibrations are obtained by the band at 1700 cm^{-1}. As a consequence, CHTC has carbonyl, ester, quinine, and carboxylic groups. This situation is supported by the wide bands at 3000–3700 cm^{-1}. C=C vibrations at 1610 cm^{-1} and aromatic C–H out-of-plane bending vibrations indicate the presence of an aromatic skeleton.[33] HS has an aliphatic structure as can be inferred from the band around 2900 cm^{-1} and these groups were also present in hydrothermally carbonized HS. The band at around 3000–3500 cm^{-1} linked with C–OH vibration and these peaks decreased in the HSHTC sample. This can be evidence of the dihydroxylation reaction in the hydrothermal carbonization.[22]

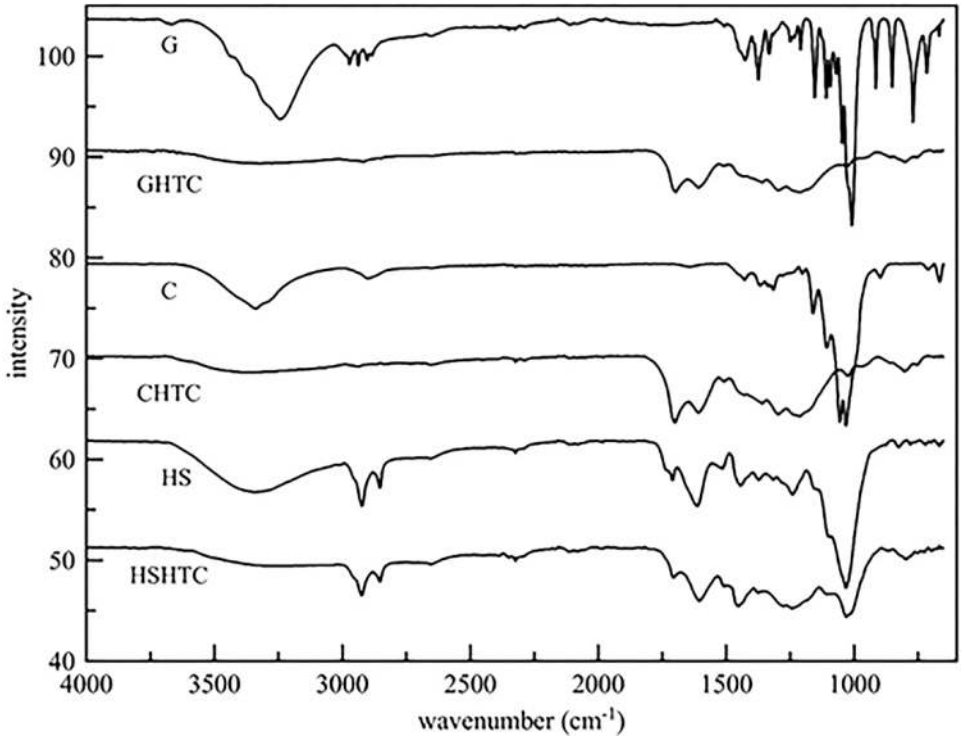

Figure 1. The FTIR spectra of the treated and untreated biomasses.

Figure 2 shows the SEM and TEM images of the biochars. The SEM images reveal the presence of perfect independent spheres with a particle diameter of about 1 μm for glucose. Particles below 100 nm can also be seen from the TEM images, indicating that the carbon structure consists of particles ranging from 50 nm to 2 μm. The sample preparation technique can cause the widening of the range due to agglomeration and aging of the carbonaceous material. The dehydration reaction of glucose leads to the formation of furfural and HMF as a product and is followed by polymerization of HMF, resulting in the formation of carbon-based spheres. The formation mechanism of the carbon-based spheres was explained in our previous study.[34]

The SEM images of CHTC and HSHTC are quite similar since hazelnut shell has a cellulose structure influencing the surface morphology. According to the SEM and TEM images of CHTC and HSHTC, the presence of spherical particles in the amorphous structure is clearly observed.

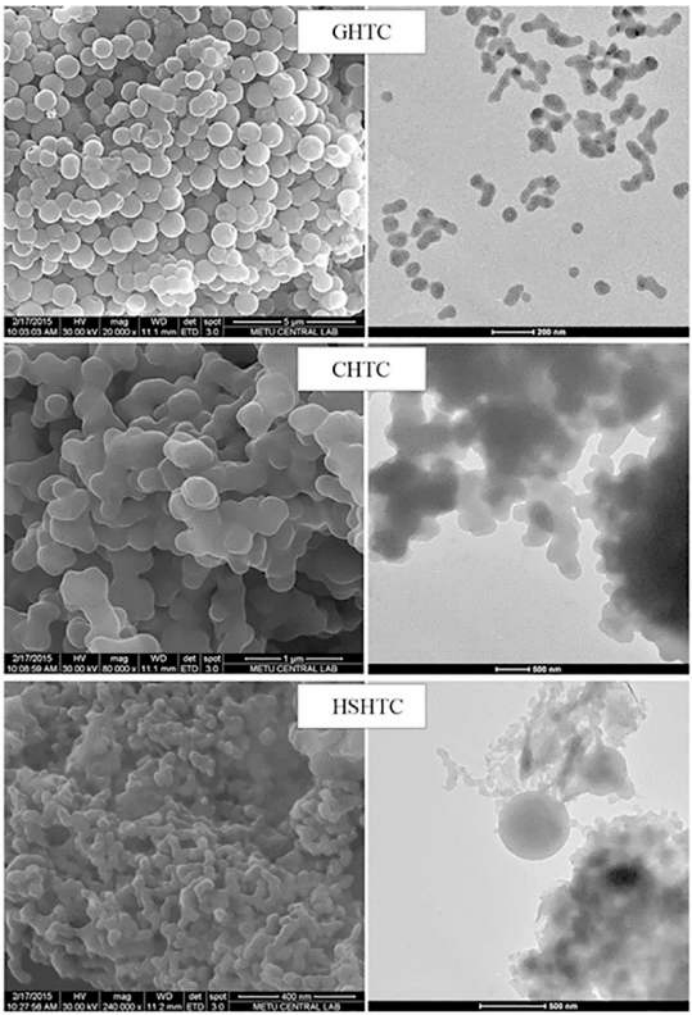

Figure 2. SEM and TEM images of glucose-, cellulose-, and hazelnut shell-based biochars.

2.3. BET analysis of biochars

The surface areas and total pore volumes of biochars are given in Table S5. The results were accordance with those reported previously.[34] BET results showed that the biomass derived adsorbents had low surface area and low total pore volume compared to the other adsorbents widely known (e.g., activated carbon). Thus, electrostatic interactions between dyes and adsorbents would be the key factor in this study.

2.4. Surface modification of biochars

The samples were coded as Biomass HTC _ SurfaceModifier. For example, GHTC _ H_2SO_4 indicates the biochar obtained from glucose and treated with H_2SO_4 after hydrothermal carbonization. Boehm titration is used for the determination of functional acidic and basic groups on the surface of activated carbon- or carbon-based biochars. For this method, $NaHCO_3$, Na_2CO_3, and NaOH are used as reactant. $NaHCO_3$ neutralizes carboxylic groups; Na_2CO_3 neutralizes carboxylic groups and lactonic groups; NaOH neutralizes carboxylic, lactonic, and phenolic groups. The concentration of surface functional groups was calculated by the following

Table. Boehm titration results of the biochars before and after surface functionalization (in mmol/g biochar).

	Carboxylic	Lactonic	Phenolic	Total acidic	Total basic
GHTC	3.0 ± 0.76	3.8 ± 0.40	5.32 ± 0.28	12.1 ± 1.44	0.4 ± 0.28
GHTC _ H_2SO_4	16.2 ± 1.12	5.6 ± 0.40	1.6 ± 1.20	23.4 ± 2.72	28.2 ± 3.56
GHTC _ HCl	1.9 ± 0.48	2.5 ± 1.64	11.3 ± 2.12	15.7 ± 4.24	1.3 ± 1.24
GHTC _ NaOH	0.0 ± 0.00	8.2 ± 1.68	5.3 ± 1.2	13.5 ± 2.88	16.8 ± 0.28
GHTC _ NH_3	9.6 ± 0.00	2.6 ± 0.32	5.0 ± 0.96	17.3 ± 1.28	3.0 ± 1.68
GHTC _ $(NH_4)_2SO_4$	0.5 ± 0.72	3.0 ± 0.40	19.7 ± 1.68	23.2 ± 2.80	10.6 ± 4.00
CHTC	1.3 ± 0.20	2.4 ± 0.36	12.2 ± 0.32	15.8 ± 0.88	0.0 ± 0.00
CHTC _ HCl	1.4 ± 0.21	0.2 ± 0.12	2.4 ± 1.04	4.0 ± 1.37	0.0 ± 1.12
CHTC _ NaOH	0.0 ± 0.24	10.7 ± 1.84	12.2 ± 1.12	23.0 ± 3.2	21.4 ± 0.84
CHTC _ NH_3	0.0 ± 0.16	1.2 ± 0.36	2.2 ± 0.53	3.4 ± 1.05	0.0 ± 0.16
CHTC _ $(NH_4)_2SO_4$	1.3 ± 0.44	4.3 ± 0.08	3.2 ± 0.52	8.8 ± 1.04	0.0 ± 0.76
HSHTC	0.0 ± 0.00	0.8 ± 0.56	1.2±0.12	2.0 ± 0.68	23.0 ± 1.4
HSHTC _ H_2SO_4	3.8 ± 2.56	3.6 ± 0.56	2.8 ± 0.0	10.2 ± 3.12	0.0 ± 0.90
HSHTC _ HCl	6.0 ± 1.60	0.6 ± 0.84	2.0 ± 0.0	8.6 ± 2.44	0.0 ± 0.90
HSHTC _ NaOH	0.0 ± 1.24	6.32 ± 0.40	7.0 ± 0.28	13.32 ± 1.92	37.8 ± 0.84
HSHTC _ NH_3	0.0 ± 0.84	3.8 ± 0.28	5.6 ± 0.56	9.4 ± 1.68	22.2 ± 1.40
HSHTC _ $(NH_4)_2SO_4$	0.0 ± 0.56	2.6 ± 0.28	3.2 ± 0.00	5.8 ± 0.84	0.0 ± 90

equation:

$$c = \frac{(\sum c_i)}{n}, \tag{1}$$

where c_i is the value of each concentration and n is the number of experiments.[35]

Boehm titration results of functionalized biochars are given in the Table. It was seen that the functionalization process affects the surface chemical composition of the biochars. It was clear that the same surface modifier had different effects on the surface of biochars, due to the different origins of the biochars. The amounts of carboxylic, lactonic, and basic groups on the surface of the glucose-based biochar increased with H_2SO_4 treatment, but it had no significant effect on the acid groups in the case of hazelnut shell. It was seen that the basic groups of biochars show great diversity in the case of real biomass.

The FTIR spectra of the biochars after surface functionalization can be seen in Figure S1 given in the Supplementary Information. For glucose-derived biochars, all functionalized samples and GHTC have similar peaks at 1600–400 cm^{-1}. This situation proves that functionalization does not disrupt the basic structure of glucose-based adsorbents. The peaks at 1042 cm^{-1} and 1172 cm^{-1} indicate the S=O stretching and asymmetric tension of the R–SO_2–OH for GHTC _ H_2SO_4. Furthermore, the intense peak at 3380 cm^{-1} can be assigned to the presence of OH groups in the sulfonic acid, proving the formation of sulfonic acid groups on the surface of GHTC _ H_2SO_4. The peak at 745–695 cm^{-1} is related to the C–Cl bonds, which was not observed for GHTC _ HCl. The phenolic structure of C–O bonds also generated bands at 1238 cm^{-1}. It is thought that the predominant peak at 3354 cm^{-1} belongs to R–OH bonds. The OH bending that appeared at 1416 cm^{-1} for GHTC _ NaOH was seen in all the spectra within different intensities. The peak at 1632 cm^{-1} is observed due to the plane bending of N–H in sample GHTC _ NH_3. It is thought that the intense peak emerging at 3354 cm^{-1} implies OH stretching as a result of NH_4OH formed from NH_3 in most of the samples. A peak at 1084 cm^{-1} arises from the S=O stretching in GHTC _ $(NH_4)_2SO_4$. The peak at 1448 cm^{-1} in the spectrum is clear evidence of the presence of C–H bending. Bands observed at 3350–3240 cm^{-1} correspond to R–NH_2 bonds.

It was observed that –NH_2 functional groups cannot be obtained from GHTC _ NH_3 in previous experiments. –NH_2 functional groups can be easily acquired using $(NH_4)_2SO_4$.

The band at 1164 cm^{-1} represents R–SO_2–OH asymmetric stretching for the sample of CHTC _ H_2SO_4. The presence of sulfonic acid groups on the surface of carbon-based material after treatment H_2SO_4 is proved. The wide peak at 3300 cm^{-1} identified in the FTIR spectrum of CHTC _ NH_3 can be assigned to N–H stretching of R_2–N–H structure.[36] Hence, unlike glucose, NH_3 and N–H groups can be attached on cellulose-based biochars. The bands at 1408 cm^{-1} identified in the IR spectra of CHTC _ $(NH_4)_2SO_4$ are assigned to SO_2 symmetric stretching in R–SO_2–OR (sulfonate group). S=O stretching bands appear at 1038 cm^{-1} for the HSHTC _ H_2SO_4 sample. The peak at 1152 cm^{-1} is due to asymmetric stretching of R–SO_2–OH. The distinctive peak at 876 cm^{-1} is assigned to S–O stretching. The FTIR spectra are very similar in HSHTC _ HCl and HSHTC. OH groups are observed only in the HSHTC _ HCl sample. According to the FTIR spectra of HSHTC _ NaOH, it can be said that NaOH breaks the structure of hazelnut shell. There is an increase in the peak at 1608 cm^{-1} attributed to C=C stretching in the HSHTC _ NH_3 sample compared to HSHTC correspondingly; there is a decline in the peak at 1700 cm^{-1} associated with C=O carbonyl groups.[37] The significant increase in peak intensity at 3378 cm^{-1} can be attributed to the presence of OH groups. The FTIR spectra of HSHTC _ $(NH_4)_2SO_4$ show an intense peak at 1130 cm^{-1} corresponding to N–C stretching. The peak at 3378 cm^{-1} can be assigned to N–H stretching. The peak at 1566 cm^{-1} is the evidence of functional groups containing nitrogen. The weak peak at 800 cm^{-1} can be assigned to S–O stretching.

2.5. Zero point of charge

The measurement of the point of zero charge of the carbon-based biochar was made according to previous studies.[38] The point of zero charge is the pH value at which the surface of biochar is globally neutral; it contains as much positively charged as negatively charged surface functions. The pH of the zero point of charge (pH_{pzc}) of biochar depends on the chemical and electronic properties of the functional groups on its surface.[39] The experimental results show that pH_{pzc} is 3.8, 3.9, and 6.4 for GHTC, CHTC, and HSTHC, respectively. This situation indicates the presence of an acidic group on the GHTC and CHTC surface. On the other hand, HSHTC surface has more basic groups. These results are supported by Boehm titration (Table). When pH rises above 4, the GHTC and CHTC surface charges become negative and electrostatic interactions are established between biochars and MB molecules. Moreover, when pH rises above 6, the same situation occurs for HSHTC. Surface charges of adsorbents become positive below their pH_{pzc} values and anionic dye adsorption increases. The opposite applies when surface charge becomes negative.

2.6. Dye adsorption performance

Figures 3, 4, and 5 show the MB adsorption capacity of glucose-, cellulose-, and hazelnut shell-derived biochars, respectively. MB adsorption of GHTC- and HSHTC-based adsorbents was very low; in contrast, the removal efficiencies for MB of CHTC-based adsorbents were increased significantly. This alignment is not compatible with the BET surface area results, since HSHTC has the maximum surface area. The adsorption of ionic dyes from aqueous solution is dependent on various factors such as structure and functional behavior of the biochars, mass transport, and electrostatic interactions.[40,41] Furthermore, it has been reported that the adsorption mechanism depends on the $\pi-\pi^*$ interactions between aromatic regions of the dye molecules and graphene-like sheets of carbon-based adsorbents.[42,43] To prove the existence of $\pi-\pi^*$ interactions in the biochars, XPS analysis is

performed (Figure S2 in Supplementary Information). According to XPS results, cellulose-derived CHTC has more $\pi-\pi^*$ transitions (delocalized electrons in the aromatic ring) than the others. As a result, an alignment for the chars as cellulose > hazelnut shell > glucose is expected depending on the XPS results. It is also expected that an increase in oxygen-containing functional groups on the surface of the biochar leads to an increase in MB adsorption. At pH values higher than 4, adsorption efficiency reached the highest value. The oxygen-containing groups attach H^+ at low pH values; thus these groups cannot reach the MB molecules. Higher pH values provide the deprotonation of carboxylic acid, which leads to an increase in adsorption capacity.[44] The results of the samples that do not have adsorption capacity are not given in the graphs to avoid confusion.

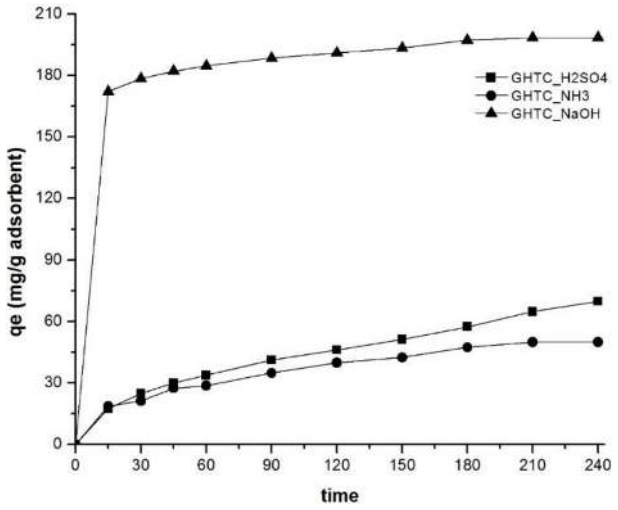

Figure 3. MB adsorption capacity of glucose derived biochars.

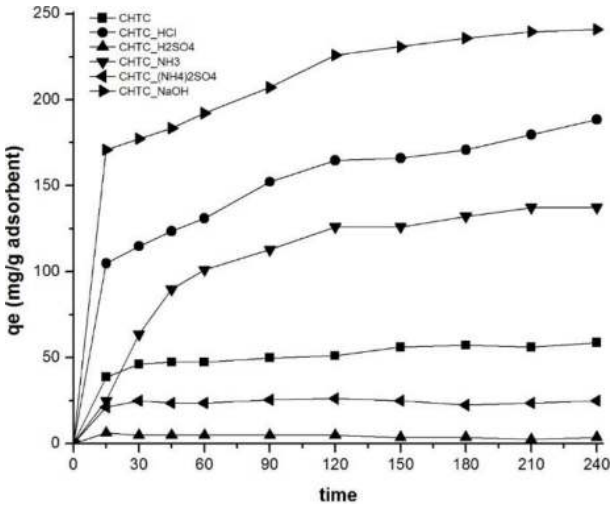

Figure 4. MB adsorption capacity of cellulose-derived biochars.

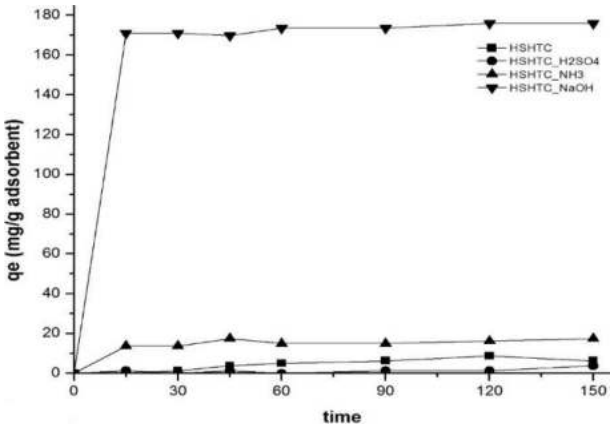

Figure 5. MB adsorption capacity of hazelnut shell-derived biochars.

GHTC _ H_2SO_4 has highest removal efficiency when compared with GHTC _ NH_3 and GHTC _ NaOH. However, bare GHTC has shown no MB adsorption (Figure 3). GHTC_ H_2SO_4 leads to a decrease in the pH of the solution. MB was adsorbed by the biochar below pH 4. The dye removal efficiency increased dramatically with increasing number of oxygen-containing functional groups on the surface and the total number of acidic groups with NH_3 and NaOH functionalization.

Adsorption of MB increased with NaOH functionalization, while a decrease in the adsorption of MB was observed with H_2SO_4 and $(NH_4)_2SO_4$ functionalization (Figure 4). The total numbers of acidic and basic groups increased with NaOH treatment as seen in the Table. The $(NH_4)_2SO_4$ treatment leads to a decrease in the number of basic groups. NaOH functionalization of biochars leads to an increase in pH (=10) and electrostatic interactions between negatively charged surfaces and positively charged dye.[45]

Almost the same adsorption efficiencies were observed for HSHT _ $(NH_4)_2SO_4$, HSHTC _ HCl and HSHTC and a small increase in HSHTC _ H_2SO_4 and a great increase in the case of HSHTC _ NaOH were observed (Figure 5). Boehm titration results show the high number of functional groups of HSHTC _ NaOH. Likewise, HSHTC _ H_2SO_4 and HSHTC _ NH_3 have a small increase in MB adsorption due to the small increase in functional groups. It can be concluded that the increase in the number of functional groups leads to a high increase in MB adsorption.

The presence of oxygen groups on the adsorbent surface is necessary for the adsorption process to take place. In addition, the number of basic groups must be greater than the number of acidic groups for MB adsorption.

Figure S3 in the Supplementary Information shows the MO adsorption capacity of glucose-derived biochars functionalized by HCl, H_2SO_4, and $(NH_4)_2SO_4$. In this case, pH of the solution and the number of acidic and basic groups on the biochar surface are important for MO adsorption. MO adsorption only occurred in GHTC _ H2SO4 due to the total number of acidic and basic groups (Table).

The surface oxygen content is closely related to the dispersibility and solubility of biochars in water. Surface-functionalized biochars should be dispersed in water since MO is a water-soluble molecule, meaning that available adsorption sites will increase and might be suitable for the aqueous phase adsorption.[46] Cellulose- and hazelnut shell-based biochars have hydrophilic oxygen-containing groups such as hydroxyl, carboxylic, and carbonyl groups. Hence, no electrostatic interaction between negatively charged biochar and MO as an anionic dye occurred. In contrast, GHTC _ H_2SO_4 either reduced the pH (pH 3) or provided the greatest electrostatic interaction with MO, resulting in the highest adsorption capacity. GHTC _ HCl, GHTC _ $(NH_4)_2SO_4$, and GHTC have a large amount of phenolic groups (Table). The OH groups lead to negatively charged biochar; thus the pH increased, resulting in a dramatic decrease in MO adsorption capacity.[47] At the same time, the presence of C=C, C=O, and C–O functional groups on the surface of GHTC proves the hydrophilic nature of GHTC (Figure 1). Cellulose- and hazelnut shell-derived and functionalized biochars showed no adsorption for MO.

2.7. Effect of auxiliaries

The real wastewater contains high dye and salt concentration; therefore, in this study, various auxiliaries were tested to investigate the effect of ionic strength on MO and MB adsorption.[28] For this purpose, 0.6 mol L^{-1} KCl, 10 mmol L^{-1} CTAB, and 0.6 mol L^{-1} $NaHCO_3$ were added to MB solution.

As stated above, NaOH-functionalized biochars have the best adsorption efficiency for MB. If the auxiliaries were used, this situation did not change. Figures S4, S5, and S6 in the Supplementary Information show the effect of the selected auxiliaries on the adsorption of MB for glucose-, cellulose-, and hazelnut shell-based biochars, respectively. In Figure S4, an alignment like GHTC _ NaOH _ KCl > GHTC _ NaOH _ CTAB > GHTC _ NaOH was obtained for MB adsorption. The adsorption capacity of MB was related to the aggregation of MB molecules. Salt ions force MB molecules to aggregate and lead to the adsorption of molecules by GHTC _ NaOH.[48] With KCl addition, dimerization of MB could be increased by electrostatic attractions;

thus the adsorption capacity of GHTC _ NaOH _ KCl is higher than that of the others. The electrostatic and hydrophobic forces between ionic dyes and ionic surfactant play an important role in dye adsorption. When the surfactant and dye have the same charge, the hydrophobic interaction will outmatch electrostatic forces.[49] As known, CTAB is a cationic surfactant and the adsorption capacities of GHTC _ NaOH _ CTAB and GHTC are similar (q_t = 199.64 and 198.39, respectively). $NaHCO_3$ is an acidic salt and, as expected, it increases the adsorption capacity of MB. CTAB and KCl increase dye adsorption efficiency for glucose-based biochars.

Figure S5 shows the effect of the selected auxiliaries on the adsorption of MB for cellulose-based biochars. The effect of CTAB and KCl on CHTC and functionalized CHTC ranged as CHTC > CHTC _ CTAB = CHTC _ KCl, CHTC _ $(NH_4)_2SO_4$_ $NaHCO_3$ > CHTC _ $(NH_4)_2SO_4$_ CTAB > CHTC _ $(NH_4)_2SO_4$ > CHTC _ $(NH_4)_2SO_4$_ KCl, CHTC _ NaOH > CHTC_ NaOH_ KCl > CHTC_ NaOH_ CTAB.

Unlike pristine glucose- and hazelnut shell-derived biochars, CTAB and KCl decreased the adsorption efficiency of MB. When ionic strength increases, adsorption increases up to a certain limit, whereafter an increase in ionic strength will decrease the adsorption capacity.[50] Thus the number of active sites on CHTC may be decreased due to electrostatic shielding by salt. In addition, K^+ ions could compete with MB molecules.[51] It is obvious that the upper limit of ionic strength was obtained for cellulose-derived biochars. $NaHCO_3$ leads to an increase in the adsorption capacity of MB.

In Figure S6, due to the decrease in pH, the adsorption capacity is decreased in the case of HSHTC and HSHTC _ KCl. In brief, CTAB and KCl additions lead to an increase in dye adsorption efficiency for hazelnut shell-based biochar in the case of functionalization with $(NH_4)_2SO_4$.

It was understood that CTAB and KCl slightly increased MB adsorption capacity except for cellulose-based biochar. Additionally, $NaHCO_3$ always increased adsorption efficiency dramatically for MB.

The adsorption capacity of MO increased for GHTC _ H_2SO_4 and the ranking is as follows: GHTC _ H_2SO_4_ KCl > GHTC _ H_2SO_4_ CTAB > GHTC _ H_2SO_4 (Figure S7 in Supplementary Information) by adding KCl and CTAB to the solution. Methyl orange has a –SO_3Na group that was ionized in acidic aqueous solution.[52] Adding KCl leads to a decrease in the pH of the methyl orange solution (pH 4), resulting in an increase in the adsorption efficiency. CTAB is a cationic surfactant that forces MO molecules and enables aggregation. Thus, KCl and CTAB increase MO adsorption for GHTC _ H_2SO_4. No adsorption of MO is observed for the cellulose- and hazelnut shell-derived biochars.

2.8. Adsorption equilibrium

Adsorption isotherms are important to understand the relationship between adsorption molecules and the liquid / solid phase in the adsorption system.[53] The adsorption data was analyzed at equilibrium of Langmuir, Freundlich and Temkin isotherms. The linear form of Langmuir isotherm equation is represented by the following equation:

$$\frac{C_e}{q_e} = \frac{1}{bQ} + \frac{C_e}{Q}, \tag{2}$$

where

q_e: The amount of adsorbate adsorbed in mg/g at equilibrium time,

C_e: The equilibrium concentration of the adsorbate ions (mg/L),

Q and b: Langmuir constants related to the maximum adsorption capacity (monolayer capacity) and energy of adsorption, respectively (b and Q are determined by the linear plot of C_e/q_e versus C_e).

R_L: The constant is used to determine the adsorption validity. The equation was invented by Webber and Chakkravorti.

$$R_L = \frac{1}{1 + bC_0}, \tag{3}$$

where

b: The Langmuir constant

C_0 (mg/L): The highest dye concentration.

R_L: Type of the isotherm to be unfavorable ($R_L > 1$), linear ($R_L = 1$), favorable ($0 < R_L < 1$), or irreversible ($R_L = 0$).

A Tempkin isotherm was developed to take into account the enthalpy of adsorption of all the molecules in solution. The Tempkin isotherm was represented by the following linear equation:[54]

$$q_e = \frac{RT}{b_T} ln A_T + \left(\frac{RT}{b_T}\right) ln C_e \tag{4}$$

A plot of q_e versus $\ln C_e$ enables the determination of the isotherm constants KT_e and bT. KT_e is the equilibrium binding constant (L/mol) corresponding to the maximum binding energy and constant bT is related to the heat of adsorption. The values of the parameters are given in Tables S1 and S2 in the Supplementary Information for MB and MO, respectively.

As seen in Tables S1 and S2, the MB adsorption of biomass-derived biochar fitted the Langmuir adsorption and the MO adsorption fitted the Temkin adsorption. Langmuir isotherms suggested that uptake occurred on the homogeneous surface by monolayer sorption without interaction between sorbed molecules because of the weak interaction forces.[55] Furthermore, the adsorption was reversible and a certain number of active regions having the same energy were situated on the biochar surface.

2.9. Kinetic study

Adsorption kinetics gave information about the retention time (contact time between adsorbent and dye). The rate constant of adsorption was determined from the first-order rate expression given by Lagergren and Svenska.[56]

$$\log (q_c - q_t) = log q_c - \left(\frac{k_1}{2.303}\right) \tag{5}$$

where q_e and q_t (mg/g) are the amounts of dye adsorbed at equilibrium and at time t (min), respectively, and k_1 (min^{-1}) is the rate constant of adsorption. Values of k_1 and q_e were calculated from the plots of q_t versus $t^{-1/2}$. By comparing R^2 values in Table S3 in the Supplementary Information, it was concluded that the adsorption data were fitted by pseudo-first-order kinetics for MO adsorption. The pseudo-second-order kinetic model was represented as follows:

$$\frac{1}{q_t} = \frac{1}{k_2 q_e^2} + \frac{t}{q_e} \tag{6}$$

where k_2 is the rate constant of second-order adsorption (g mol^{-1} min^{-1}). The plot of t/q_t versus t showed a linear relationship and it was decided that MB adsorption was a proper pseudo-second-order model. This result was supported by R^2 values ($R^2 > 0.99$) (Table S4 in Supplementary Information).

3. Experimental

Cellulose (microcrystalline, Sigma Aldrich), glucose (D-(+) glucose monohydrate, Sigma Aldrich), methylene blue (Sigma Aldrich), methyl orange (Sigma Aldrich), potassium chloride (KCl, Sigma Aldrich), sodium bicarbonate ($NaHCO_3$, Sigma Aldrich), cetyl trimethyl ammonium bromide (CTAB, Sigma Aldrich), sodium carbonate Na_2CO_3, Sigma Aldrich), and sodium hydroxide (NaOH, Sigma Aldrich) were used without further purification. Hazelnut shell samples were dried and milled down to 425 μm.

3.1. Preparation of biochars

The hydrothermal carbonization process was carried out in a Parr autoclave system with a liter internal volume. Experiments were performed with 200 g/L glucose at 220 °C for 6 h (for 100 g/L cellulose at 220 °C, 4 h; for 100 g/L hazelnut shells at 260 °C, 6 h). A specified amount of biomass and deionized water were added to the autoclave and the autoclave was heated to the determined temperature. The experiments were carried out at 4 °C/min heating rate. After the specified time for each experiment at the desired temperature, the autoclave was cooled down to room temperature and the slurry mixture was removed. The solid products were collected by vacuum filtration and rinsed with deionized water and ethyl alcohol three times to remove the impurities. To obtain the final products, rinsed solid particles were dried in an oven at 80 °C for 24 h.

3.2. Characterization

FTIR analysis was performed with a Thermo Scientific Nicolet IS10. The Brunauer–Emmett–Teller (BET) N_2 adsorption of the particles was determined by Quantachrome NOVA 2200 series volumetric gas adsorption instrument. The total pore volume was found from the NLDFT kernel at the relative pressure of 0.99. XPS analysis was performed using a PHI 5000 VersaProbe. Boehm titrations were performed as described previously.[35] The pH at point zero charge (pHpzc) of adsorbents was measured as given in Liu's study.[57] The surface charge of the samples was determined by measuring the zeta potential (ζ) of biochars according to the procedure described by Johnson et al.[58]

3.3. Surface modification

The surface functionalization of biochars was performed successfully using various surface modification agents to increase the oxygen content of surfaces. Carbon-based biochars were treated with acid (H_2SO_4, HCl), base (NaOH, NH_3), and $(NH_4)_2SO_4$ salt. The experiments were carried out in a two-necked flask with a reflux condenser placed on a heater with a magnetic stirrer. The carbon-based biochars were seen to disintegrate in acidic medium at 80 °C. 1 M 100 mL of the modification agent and 1 g of carbon-based biochars were transferred into a flask and held at 60 °C for 4 h. At the end of the 4 h, the product was filtered under vacuum and dried in an oven at 80 °C for 24 h.

3.4. Adsorption studies

The aqueous solutions of MB with 10 ppm and MO with 20 ppm initial concentrations were prepared for the adsorption studies. The adsorption studies were conducted with 10 mg of biochar for MB solutions and 150 mg for MO solutions. Prior to each experiment, the suspension was magnetically stirred in the dark for 240 min in order to establish an adsorption–desorption equilibrium state. At given time intervals, analytical samples were taken from the suspension and immediately centrifuged for 5 min and the filtrate was analyzed by UV-Vis

spectrophotometer. The amount of dye molecules adsorbed per unit mass of the biochar was calculated with Eq. (7).

$$q_t = \frac{(C_0 - C_e)\,V}{m}, \tag{7}$$

where q_t is the adsorption capacity of the biochar (mg/g), C_0 is the initial concentration and C_e is the equilibrium concentration of dye solution (mg/L), V is the volume of the dye solution (L), and m is the mass of the biochar used (g).

4. Conclusion

The development of adsorption capacity was performed by surface functionalization of biochars with H_2SO_4, HCl, NaOH, NH_3, and $(NH_4)_2SO_4$. Surface functionalization leads to an increase in oxygen-containing functional groups on the surface. Surface functional groups and $\pi - \pi^*$ interactions in the structure of biochar are effective factors for adsorption capacity. Selected auxiliaries have significant effects on the pH of the solution, structure of the dye, and electrostatic interactions between the dye and biochar. By investigating the adsorption mechanism, proper biochars with desired surface properties can be synthesized and/or modified by different agents. Salts could be used to improve the adsorption capacity of biochars.

Acknowledgment

The authors express their thanks to the Scientific and Technological Research Council of Turkey (TÜBİTAK) for its financial support under project number KBAG-113Z635.

References

1. Rafatulla, M.; Sulaiman O.; Hashim, R.; Ahmad, A. *J. Hazard. Mater.* **2010**, *177*, 70 -80.
2. Danwittayakula, S.; Jaisaib, M.; Dutta, J. *Appl. Catal. B-Environ.* **2015**, *163*, 1-8.
3. Liu, Y.; Xu, D.; Wang, P.; Dong, Y. *Desalination and Water Treatment* **2016**, *57*, 6772-6780.
4. Dalhatou, S.; Pétrier, C.; Laminsi, S, Baup, S. *J. Environ. Technol.* **2015**, *12*, 35-44.
5. Yang, C.; Li, L.; Shi, J.; Long, C.; Li, A. *J. Hazard. Mater.* **2015**, *284*, 50-57.
6. Chiappisi, L.; Simon, M.; Gradzielski, M. *ACS Appl. Mater. Interfaces* **2015**, *7*, 6139-6145.
7. Deng, S. J.; Wang, R.; Xu, H. J.; Jiang, X. S.; Yin, J. *Mater. Chem.* **2012**, *22*, 10055-10061.
8. Thiam, A.; Sirés, I.; Garrido, J. A.; Rodríguez, R. M.; Brillas, E. *Sep. Purif. Technol.* **2015**, *140*, 43-52.
9. Demierege, S.; Toptas, A.; Ayan, E. M.; Yasa, I.; Yanik, J. *Chem. Ecol.* **2015**, *31*, 1-14.
10. Kadama, A. A.; Ladeb, H. S.; Leea, D. S.; Govindwar, S. P. *Bioresource Technol.* **2015**, *176*, 38-46.
11. Punzia, M.; Anbalagana, A.; Börnera, R. A.; Svensson, B. M.; Jonstrupa, M.; Mattiasson, B. *Chem. Eng. J.* **2015**, *270*, 290-299.
12. Manenti, D. R.; Soares, P. A.; Módenes, A. N.; Espinoza-Quiñones, F. R.; Boaventura, R. A. R.; Bergamasco, R.; Vilar, V. J. P. *Chem. Eng. J.* **2015**, *266*, 203-212.
13. Chen, Q.; Yang, Y.; Zhou, M.; Liu, M.; Yu, S.; Gao, C. *J. Hazard. Mater.* **2015**, *284*, 121-129.
14. Ahmad, M.; Lee, S. S.; Dou, X.; Mohan, D.; Sung, J. K.; Yang, J. E.; Ok, Y. S. *Bioresource Technol.* **2012**, *118*, 536-544.
15. Lu, H.; Zhang, W.; Yang, Y.; Huang, X.; Wang, S.; Qui, R. *Water. Res.* **2012**, *46*, 854-862.

16. Karakoyun, N.; Kubilay, S.; Aktas, N.; Turhan, O.; Kasimoglu, M.; Yilmaz, S.; Sahiner, N. *Desalin. Water Treat.* **2011**, *280*, 319-325.
17. Zheng, W.; Guo, M.; Chow, T.; Bennett, D. N.; Rajagopalan, N. *J. Hazard. Mater.* **2010**, *181*, 121-126.
18. Cao, X.; Ma, L.; Gao, B.; Harris, W. *Environ. Sci. Technol.* **2009**, *43*, 3285-3291.
19. Qian, L.; Chen, B. *Environ. Sci. Technol.* **2013**, *47*, 8759-8768.
20. Xu, X.; Cao, X.; Zhao, L. *Chemosphere* **2013**, *92*, 955-961.
21. Shen, Y. S.; Wang, S. L.; Tzou, Y. M.; Yan, Y. Y.; Kuan, W. H. *Bioresource Technol.* **2012**, *104*, 165-172.
22. Donar, Y. O.; Çağlar, E.; Sınağ, A. *Fuel* **2016**, *193*, 366-372.
23. Sinag, A.; Yumak, T.; Balci, V.; Kruse, A. *J. Supercrit. Fluids* **2011**, *56*, 179-185.
24. Sinag, A.; Kruse, A.; Maniam, P. *ACS Sym. Ser.* **2012**, *71*, 80-85.
25. Schumacher, M.; Yanık, J.; Sinag, A.; Kruse, A. *ACS Sym. Ser.* **2011**, *58*, 131-135.
26. Liu, Y.; Zhao, X.; Li, J.; Ma, D.; Han, R. *Desalin. Water Treat.* **2012**, *46*, 115-123.
27. Sevilla, M.; Fuertes, A. B. *Carbon* **2009**, *47*, 2281-2289.
28. Cimino, G.; Passerini, A.; Toscano, G. *Water Research* **2000**, *34*, 2955-2962.
29. Kang, S.; Li, X.; Fan, J.; Chang, J. *Ind. Eng. Chem. Res.* **2012**, *51*, 9023-9031.
30. Unur, E. *Micropor. Mesopor. Mat.* **2013**, *168*, 92-101.
31. Latham, K. G.; Jambu, G.; Joseph, S. D.; Donne, S. W. *ACS Sus. Chem. Eng.* **2013**, *27*, 755-764.
32. Oliveira, P. R.; Lamy-Mendes, A. C, Rezende, E. I. P.; Mangrich, A. S.; Junior, L. H. M.; Bergamini, M. F. *Food Chem.* **2015**, *171*, 426-431.
33. Liu, L.; Gao, Z. Y.; Su, X. P.; Chen, X.; Jiang, L.; Yao, J. M. *ACS Sus. Chem. Eng.* **2015**, *3*, 432-442.
34. Aydincak, K.; Yumak, T.; Sinag, A.; Esen, B. *Ind. Eng. Chem. Res.* **2012**, *51*, 9145-9152.
35. Huff, M. D.; Kumar, S.; Lee, J. W. *J. Environ. Manage.* **2014**, *146*, 303-308.
36. Qui, Y.; Zheng, Z.; Zhou, Z.; Sheng, G. D. *Bioresour. Technol.* **2009**, *100*, 5348-5351.
37. Leng, L.; Yuan, X.; Zeng, G.; Shao, J.; Chen, X.; Wu, Z.; Wang, H.; Peng, X. *Fuel* **2015**, *155*, 77-85.
38. Liu, Y.; Zhao, X.; Li, J.; Ma, D.; Han, R. *Desalin. Water Treat.* **2012**, *46*, 115-123.
39. Solpan, D.; Duran, S.; Saraydin, D.; Güven, O. *Phys. Chem.* **2003**, *66*, 117-127.
40. Ma, J.; Yu, F.; Zhou, L.; Jin, L.; Yang, M.; Luan, J.; Tang, Y.; Fan, H.; Yuan, Z. Chen J. *ACS Appl. Mater. Interfaces.* **2012**, *4*, 5749-5760.
41. Xu, R.; Xiao, S.; Yuan, J.; Zhao, A. *Bioresource Technology.* **2011**, *102*, 10293-10298.
42. Al-Degs, Y. S.; El-Barghouthi, M. I.; El-Sheikh, A. H.; Walker, G. A. *Dyes. Pigments.* **2008**, *77*, 16-23.
43. Zaghbani, N.; Hafiane, A.; Dhahbi, M. *Sep. Purif. Technol.* **2007**, *55*, 117-124.
44. Alberghina, G.; Bianchini, R.; Fichera, M.; Fisichella, S. *Dyes. Pigments* **2000**, *46*, 129-137.
45. Li, M.; Wang, S.; Luo, W.; Xia, H.; Gao, Q.; Zhou, C. *J. Chem. Technol. Biot.* **2015**, *90*, 1124-1134.
46. Mahanta, D.; Madras, G.; Radhakrishnan, S.; Patil, S. *Phys. Chem. B* **2008**, *112*, 10153-10157.
47. Wang, S.; Boyjoo, Y.; Choueib, A. A. *Chemosphere* **2005**, *60*, 1401-1407.
48. Hameed, B. H.; Ahmad, A. A. *J. Hazard. Mater.* **2009**, *164*, 870-875.
49. Kavithaa, D.; Namasivayam, C. *Bioresource Technology* **2007**, *98*, 14-21.
50. Hameed, B. H.; Ahmad, A. L.; Latiff, K. N. A. *Dyes Pigments* **2007**, *75*, 143-149.
51. Hamdaoui, O. *J. Hazard. Mater.* **2006**, *135*, 264-273.

52. Ho, Y. S.; Ng, J. C. Y.; McKay, G. *Separ. Purif. Method.* **2000**, *29*, 189-232.
53. Detwiler, M. D.; Milligan, C. A.; Zemlyanov, D. Y.; Delgass, W. N., Ribeiro, F. H. *Surf. Sci.* **2016**, *648*, 220-226.
54. Liu, Y. *Colloid Surface A* **2006**, *274*, 34-36.
55. Nigri, E.; M, Bhatnagar, A.; Rocha, S. D. F. *J. Clean. Prod.* **2016,** *274*, 34-36.
56. Liu, Y.; Zhao, X.; Li, Jianli.; Ma, Dan.; Han, R. *Desalin. Water Treat.* **2012**, *46*, 1-3.
57. Johnson, P.; R., Sun, N.; Elimelech, M. *Env. Sci. Tech.* **1996**, *30*, 3284-3293.

Supporting Information

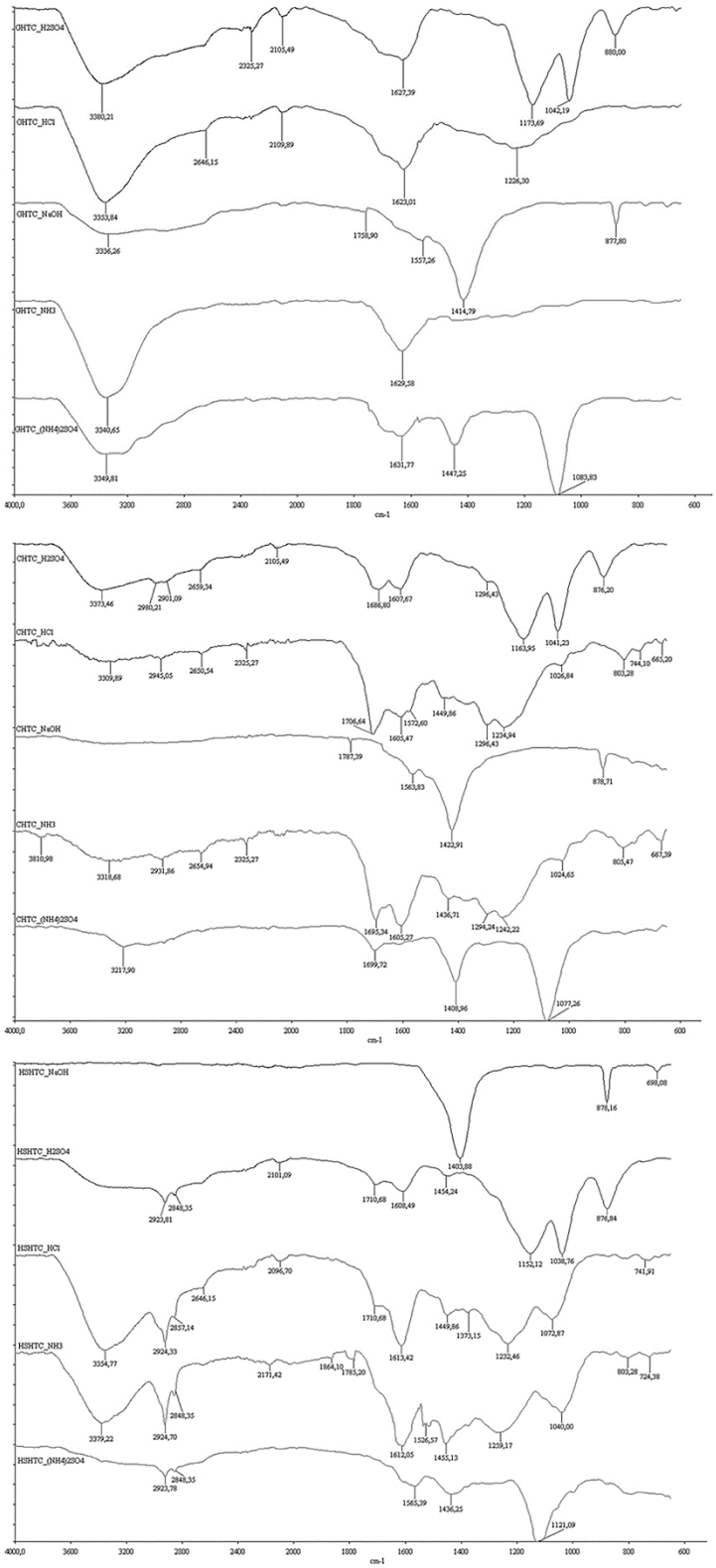

Figure S1. FTIR spectra of glucose-, cellulose-, and hazel nut shell-based and surface-functionalized biochars.

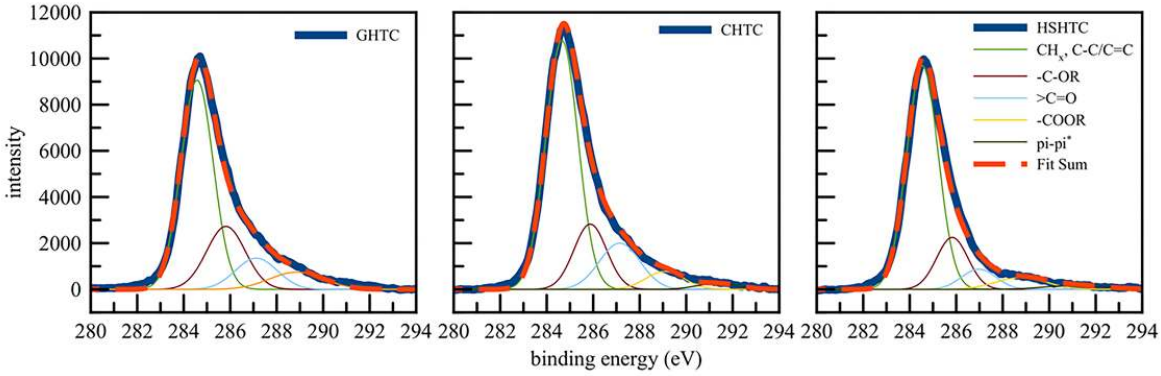

Figure S2. XPS analysis of biomass-derived biochars.

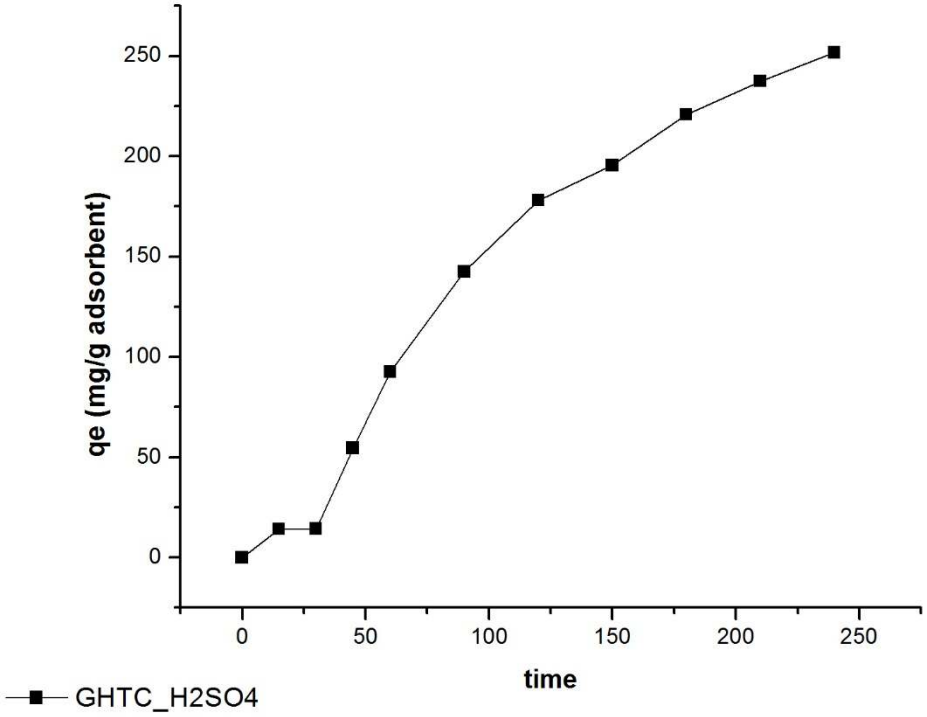

Figure S3. MO adsorption capacity of glucose-derived biochars.

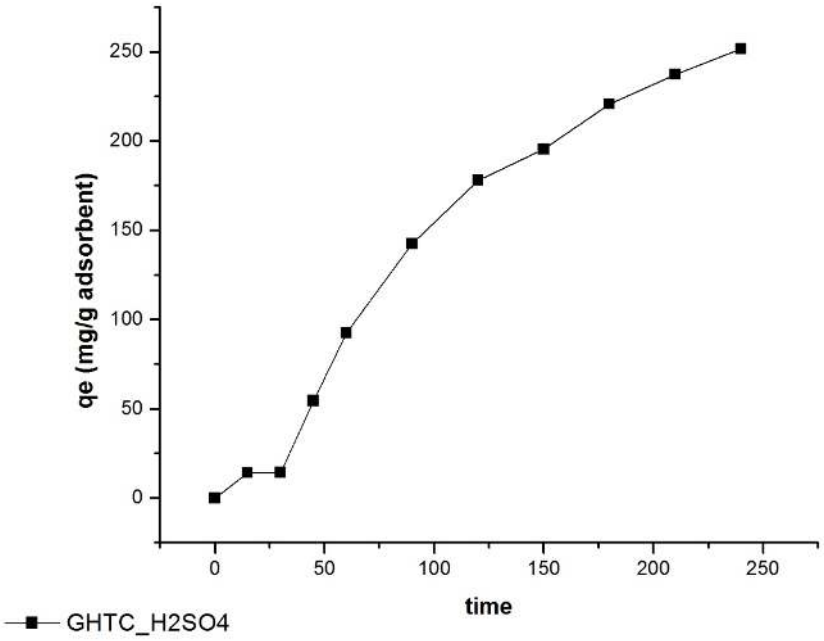

Figure S4. Effect of CTAB, KCl, and $NaHCO_3$ on the adsorption of MB for glucose-derived biochars.

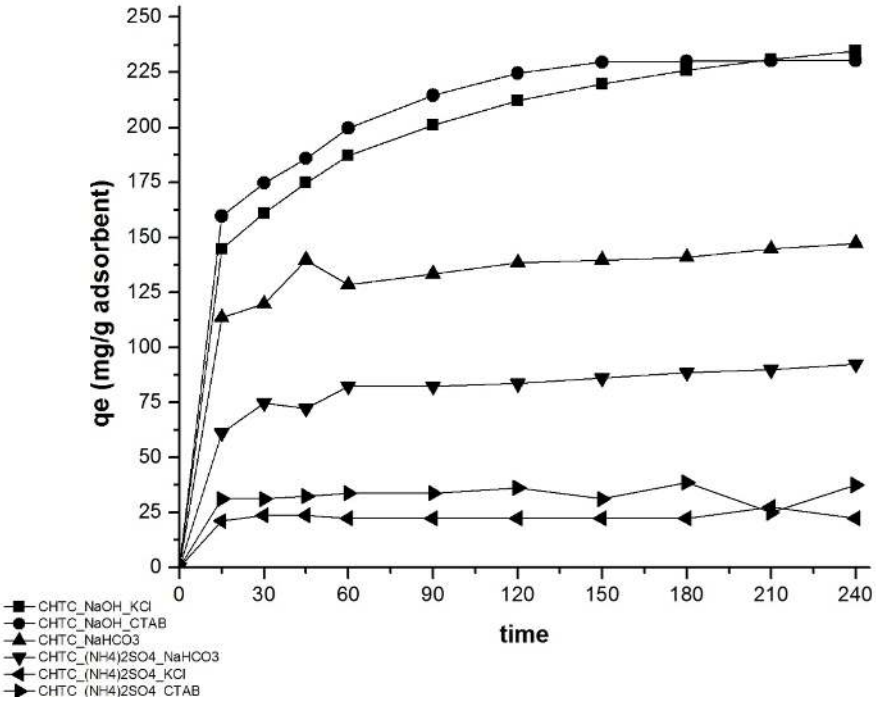

Figure S5. Effect of CTAB, KCl, and $NaHCO_3$ on the adsorption of MB for cellulose-derived biochars.

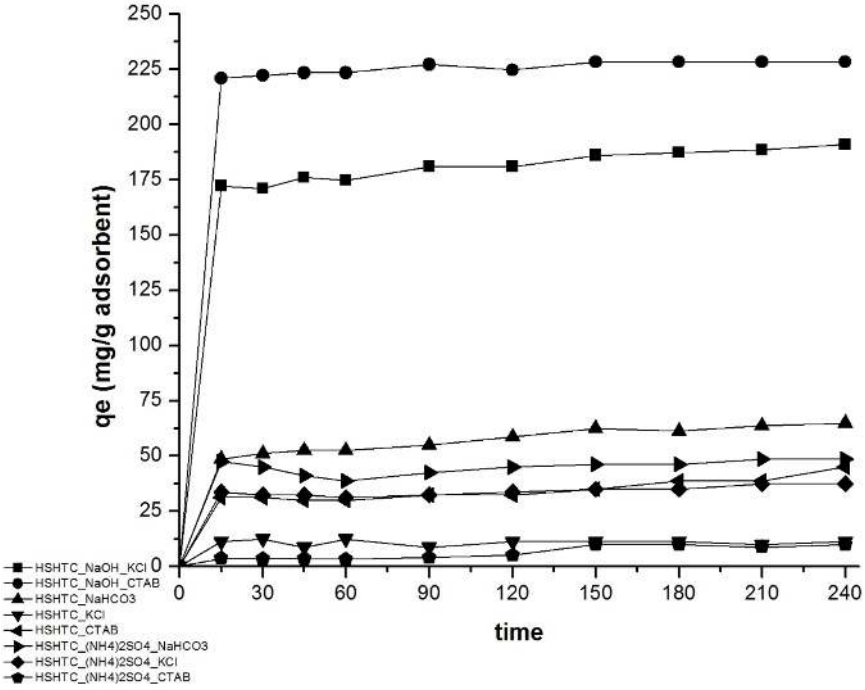

Figure S6. Effect of CTAB, KCl, and $NaHCO_3$ on the adsorption of MB for hazelnut shell-derived biochars.

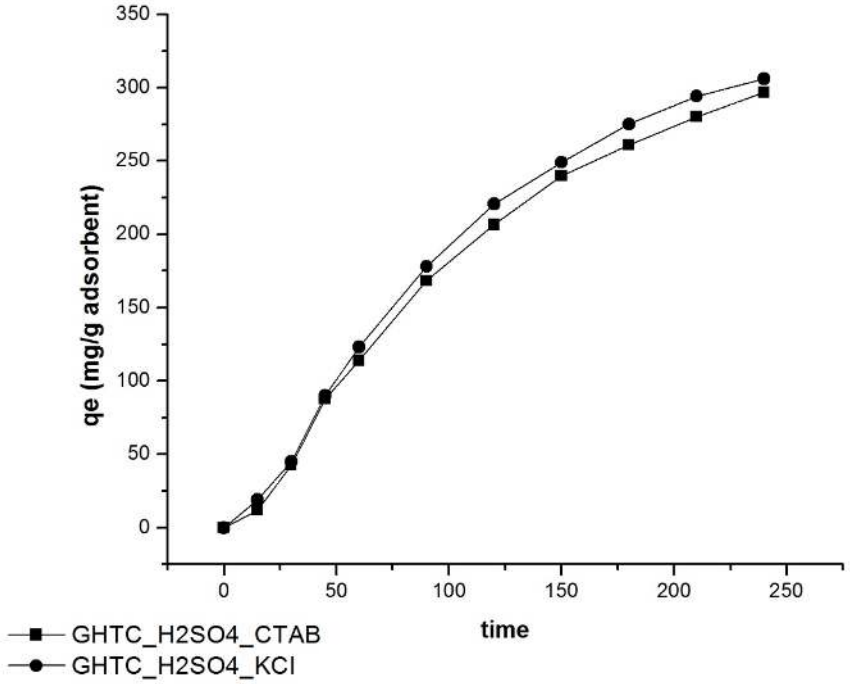

Figure S7. Effect of CTAB, KCl, and $NaHCO_3$ on the adsorption of MO for glucose-derived biochars.

Table S1. Langmuir isotherm parameters for the adsorption of MB.

Sample ID	b (L / mg)	Q_{max} (mg / g)	R^2	R_L
GHTC _ NaOH	2.31	149.25	0.9982	0.036
GHTC _ NaOH _ KCl	2.63	158.73	0.9993	0.0031
GHTC _ NaOH _ CTAB	2.19	147.05	0.9975	0.038
CHTC _ NaOH	11.4	175.44	0.9941	$7.23x10^{-3}$
CHTC _ NaOH _ KCl	1.97	140.85	0.9826	0.039
CHTC _ NaOH _ CTAB	12	166.66	0.9910	$7.13x10^{-3}$
HSHTC _ NaOH	1.19	126.58	0.9999	0.066
HSHTC _ NaOH _ KCl	0.60	114.94	0.9994	0.108
HSHTC _ NaOH _ CTAB	1.96	181.82	0.9999	0.035

Table S2. Tempkin isotherm parameters for the adsorption of MO.

Sample ID	K_{Te} (L/g)	b_T (J/mol)	R^2
GHTC _ H_2SO_4	0.871	170.96	0.9889
GHTC _ H_2SO_4 _ CTAB	0.929	214.63	0.976
GHTC _ H_2SO_4 _ KCl	0.936	222.16	0.9744

Table S3. Kinetic parameters of pseudo-first-order and pseudo-second-order models for the adsorption of MB onto biomass derived biochars.

	Pseudo-first-order model			Pseudo-second-order model		
Sample ID	k_1 (min^{-1})	qe (mg/g)	R^2	k_2 (g/mg min)	qe (mg/g)	R^2
GHTC _ NaOH	0.0086	1.7751	0.8232	0.005	0.0236	0.9997
GHTC _ NaOH _ KCl	0.0073	1.6405	0.7921	0.0049	0.0172	0.9998
GHTC _ NaOH _ CTAB	0.0074	1.8245	0.8601	0.0049	0.0306	0.9994
CHTC _ NaOH	0.0079	2.1492	0.9457	0.0039	0.0589	0.9978
CHTC _ NaOH _ KCl	0.0071	2.1643	0.9644	0.004	0.0704	0.9983
CHTC _ NaOH _ CTAB	0.0143	2.2772	0.9785	0.0041	0.045	0.994
HSHTC _ NaOH	0.0157	1.5002	0.5391	0.0056	0.0069	0.9999
HSHTC _ NaOH _ KCl	0.0063	1.6559	0.7659	0.0052	0.024	0.9995
HSHTC _ NaOH _ CTAB	0.0117	1.4727	0.4956	0.0044	0.0051	0.9999

Table S4. Kinetic parameters of pseudo-first-order and pseudo-second-order models for the adsorption of MO onto biomass derived biochars.

	Pseudo-first-order model			Pseudo-second-order model		
Sample ID	k_1 (min^{-1})	qe (mg/g)	R^2	k_2 (g/mg min)	qe (mg/g)	R^2
GHTC _ H_2SO_4	0.0062	2.5619	0.984	0.0036	1.4524	0.2504
GHTC _ H_2SO_4 _ CTAB	0.006	2.607	0.9789	0.0003	0.7308	0.0094
GHTC _ H_2SO_4 _ KCl	0.0066	2.6459	0.9639	0.0005	0.5663	0.1213

Table S5. Zeta potential and surface analysis of biochars.

	pH	Zeta pot. (mV)	BET N_2 surface area ($m^2\ g^{-1}$)	Pore volume ($cc\ g^{-1}$)
GHTC	3.2	+11.2	5.44	0.0312
CHTC	5.8	−26.4	12.87	0.0846
HSHTC	6.8	−12.4	23.01	0.0656